Dynamic Analysis of a 6 DOF CKCM Robot End-effector for Dual-arm Telerobot Systems *

Charles C. Nguyen [†] and Farhad J. Pooran [‡]

Center for Artificial Intelligence and Robotics, School of Engineering and Architecture, The Catholic University of America, Washington DC, 20064, USA

In this paper, we present the dynamical analysis of a six-degree-of-freedom robot end-effector built to study telerobotic service and maintenance of NASA hardwares in space. The design of the end-effector is based on the concept of closed-kinematic chain mechanism capable of performing precise motion in a small workspace. After presenting a closed-form solution for the inverse kinematic problem, we employ the Lagrangian approach to derive a set of equations of motion for the end-effector where the generalized coordinates are selected to be the Cartesian coordinates. Computer simulation study shows that the centrifugal and Coriolis terms can be neglected for slow motion. Effects of system parameters on the end-effector dynamics are also studied using computer simulation.

Dr. Charles C. Nguyen received the degree of Diplom Ingenieur in Electrical Engineering at Konstanz Technical University, West Germany where he was also named *"Best Graduate of the Class of 1978,"* in 1978. Later he earned his Master of Science in 1980 and Doctor of Science in 1982 both with honor at the George Washington University. He joined the Catholic University of America in 1982 at the rank of Assistant Professor and was promoted to Associate Professor in 1987, a position he still holds. Since 1985 he has been the Director of the Center for Artificial Intelligence and Robotics at Catholic University of America.

Professor Nguyen has published numerous technical and scientific papers in the area of control and robotics in major technical journals such as *IEEE Transactions of Automatic Control* and *International Journal of Control.* He also presented research papers at several international conferences.

Dr. Nguyen is a member of IEEE, ISMM, Sigma Xi, and a member and Chief Faculty Advisor of Tau Beta Pi Engineering Honor Society. He is also a member of The Research Board of Advisors of American Biographical Institute and International Biographical Centre. He was the recipient of the "Research Initiation Award" from Engineering Foundation in 1986 and was awarded NASA/ASEE Fellowship Awards in 1985 and 1986. Recently he was the recipient of the "Academic Vice President Research Excellence Award," in February 1989 from the Catholic University of America. His life and achievements are listed in 18 biographical registers and Who's Who.

His research interests lie in the areas of time-varying control systems, control of large space structures, decentralized control, control of robot manipulators, robot vision and neural networks. His research has been continuously supported by several agencies including NASA and Engineering Foundation. He is also a consultant in the area of control and robotics for local companies and government agencies. He is currently the principal investigator of 2 research grants funded by NASA/Goddard Space Flight Center in the areas of autonomous robots and telerobotics.

Farhad J. Pooran received his B.S. and M.S. degrees in Mechanical Engineering from Arya-Mehr University of Technology, Tehran, Iran in 1977 and 1979, respectively. He has currently completed his Ph.D. degree in Mechanical Engineering at the Catholic University of America, Washington, DC.

From 1980 to 1984, he worked as a plant engineer in Abyek Cement Plant in Iran. Since 1986 he has been a Research Assistant in the Center for Artificial Intelligence and Robotics at the Catholic University of America. He has been involved with NASA sponsored research in the area of robotics and control and has published several journal and conference papers in this research area.

His research interests include kinematics, dynamics, control, and design of robot manipulators.

1. Introduction

Realizing that space operations such as servicing and maintaining spacecrafts are dangerous, NASA has focused its attention on the research of *telerobotics*, a combination of *teleoperation* and *robotics* [1]. During the *trade control mode* of a telerobotic operation, using teleoperation the human operator performs some portion of a task and then let the telerobot perform some other portions of the task autonomously. A telerobot system mainly consists of a master arm and two slave arms each of which is usually an open-kinematic chain (OKC) manipulator possessing 6 degrees of freedom (DOF) or more (*Fig. 1*). Robotic assembly such as fastening and mating of parts requires very high precision motion. Therefore, in order to achieve a successful assembly task, it is envisioned that during a traded control mode, the operator uses the master arm to move the slave arms into the assembly workspace and then an end-effector which is to be mounted to the end of each slave arm and capable of performing precise motion, will take over and perform the assembly task autonomously.

The cantilever-like structure of OKC manipulators causes the manipulator arm to have low stiffness, which results in a serial accumulation of the link errors. Consequently, although OKC manipulators have large workspace and high dexterity, they are not utilized in tasks requiring high precision positioning. Drawbacks of OKC manipulators has motivated researchers to seek an alterna-

tive type of manipulators whose design is based on the concept of *closed-kinematic chain mechanism* (CKCM). Compensating for a relatively small workspace and low maneuverability, CKCM manipulators are capable of high precision positioning due to their high structural rigidity and noncumulative link errors. In addition, CKCM manipulators have higher strength-to-weight ratios as compared to OKC manipulators because their actuators share the payload proportionally. Implementation of the CKCM concept first appeared in the design of the Stewart platform mechanism [2], originally implemented as an aircraft simulator. Later the Stewart platform concept was considered in many robotic applications [3]–[5]. Modified versions of the Stewart platform were developed in [6] and [7]. Application of linear algebra elements to screw systems was considered in [8] to describe the instantaneous link motion of a single closed-loop mechanism. Research in [6] focused on the structural kinematic problem of in-parallel manipulators. Application of Stewart platform into the implementation of a passive compliant robot and-effector was considered in [9]. The authors in [10] and [7] investigated the kinematic problem and practical construction of the Stewart platform, respectively. Inverse dynamic problem of platform-based manipulators was studied in [11] and analysis of kinematics and dynamics of parallel manipulators was conducted in [12]. Using Lagrangian formulation, dynamical equations were derived for a 3 DOF CKCM manipulator in [13] and for a 2 DOF CKCM manipulator in [14].

MASTER SYSTEM
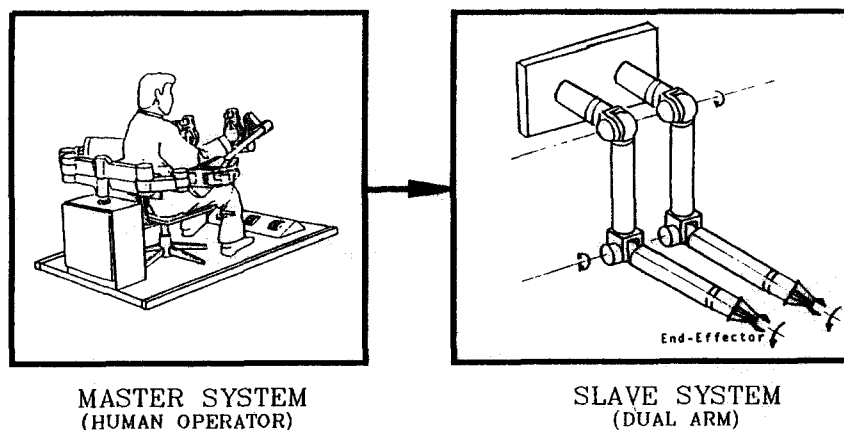(HUMAN OPERATOR)

SLAVE SYSTEM
(DUAL ARM)

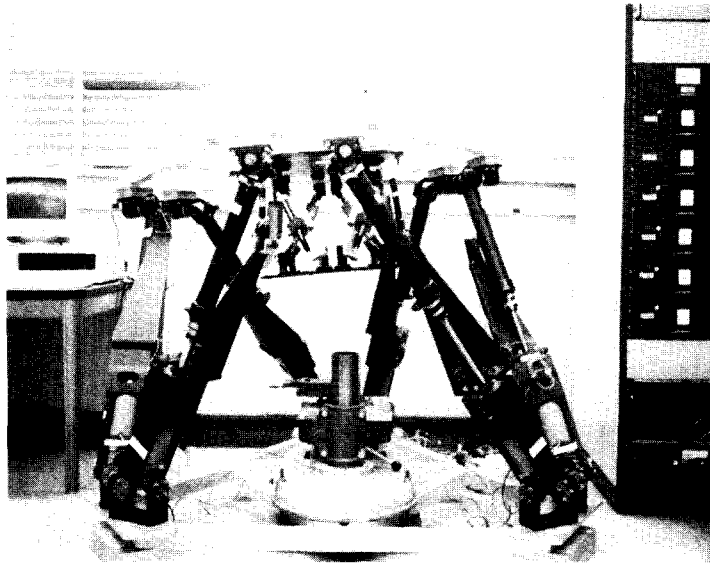Fig. 1. A dual-arm telerobot system with CKCM end-effectors.

Fig. 2. The CKCM end-effector.

Research work in [15] analyzed the kinematics problem of a 6 DOF CKCM end-effector whose workspace determination was also investigated.

Based on the fact that CKCM manipulator can provide high precision motion in a limited workspace, a 6 DOF robot end-effector whose design is based on the Stewart platform mechanism, was built to serve as a testbed for studying telerobotic assembly of NASA hardwares in space [9]. This paper presents the dynamical analysis of the above end-effector. We first describe the construction of the end-effector in the next section. After that, a closed-form solution to its inverse kinematic problem is presented. We then apply Lagrangian approach to derive the dynamical equations which are later simplified by neglecting centrifugal and Coriolis effects by using computer simulation. Finally, effects of system parameters on the end-effector dynamics are studied by computer simulation.

2. The 6 DOF CKCM End-effector

In order to study the performance of autonomous assembly of parts in a telerobotic operation, a 6 DOF end-effector whose size is about ten times that of the end-effector which is to be mounted to the slave arms of the telerobot systems was designed and built at the Goddard Space Flight Center (GSFC) [9] and is currently located at the Center for Artificial Intelligence and Robotics * (CAIR). As shown in *Fig. 2*, the end-effector is a modified version of the Stewart platform, and mainly consists of an upper payload platform, a lower base platform and six linear actuators. The movable payload platform is supported above the stationary base platform by six axially extensible rods where recirculating ballscrews are used to provide the extensibility. Stepper motors were selected to drive the ballscrews to extend or shorten the actuator lengths whose variations will in turn produce the motion of the payload platform. Each end of the actuator links is mounted to the platform by 2 rotary joints whose axes intersect and are perpendicular to each other. Therefore, the system has 24 rotary joints, 6 prismatic joints, and 14 links including the 2 platforms. *Number synthesis* [4] can be employed to prove that the CKCM end-effector possesses 6 degrees of freedom.

---

* To test control schemes developed under a research grant.

3. Dynamical Modeling of the End-effector

In this section we first present the inverse kinematic solution for the end-effector and then derive the equations of motion by applying the Lagrangian formulation.

3.1. The Inverse Kinematics

Inverse kinematics deals with the determination of a set of joint variables, which yield a set of Cartesian variables, usually composed of Cartesian position and orientation of the end-effector with respect to some reference frame. For the CKCM end-effector, the lengths of the links can be adjusted by the actuators, and therefore are chosen to be the joint variables. To define the Cartesian variables we proceed to assign two coordinate frames $\{A\}$ and $\{B\}$ to the movable and base platforms, respectively. As *Fig. 3* illustrates, the Origin of Frame $\{A\}$ is chosen to be the centroid A of the payload platform, the z-axis is pointing upward and the x-axis passes through the joint attachment point A_i. The angle between A_1 and A_2 is denoted by θ_A, and in order to obtain a symmetrical distribution of joints on the payload platform the angles between A_1 and A_3 and between A_3 and A_5 are set to 120°. Similarly, Frame $\{B\}$ has its origin at the centroid B of the base platform. The x-axis passes through the joint attachment point B_1 and the angle between B_1 and B_2 is denoted by θ_B. Also the angles between B_1 and B_3 and between B_3 and B_5 are set to 120°
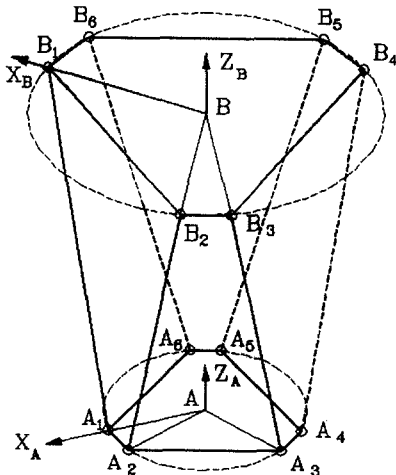

Fig. 3. Platform frame assignment.

so that a symmetrical distribution of joints on the base platform can be achieved. The Cartesian variables are chosen to be the relative position and orientation of Frame $\{A\}$ with respect to Frame $\{B\}$ where the position of Frame $\{A\}$ is specified by the position of its origin with respect to Frame $\{B\}$. Now if we denote the angle between AA_i and x_A by λ_i and the angle between BB_i and x_B by Λ_i for $i = 1, 2, \ldots, 6$ then by inspection, we obtain

$$\Lambda_i = 60(i - 1) \text{ deg.}; \qquad \lambda_i = 60(i - 1) \text{ deg.},$$
$$\text{for } i = 1, 3, 5 \tag{1}$$

and

$$\Lambda_i = \Lambda_{i-1} + \theta_B \text{ deg.}; \qquad \lambda_i = \lambda_{i-1} + \theta_A \text{ deg.},$$
$$\text{for } i = 2, 4, 6. \tag{2}$$

Furthermore, if Vector ${}^A a_i = (a_{ix} a_{iy} a_{iz})^T$ describes the position of the attachment point A_i with respect to Frame $\{A\}$, and Vector ${}^B b_i = (b_{ix} b_{iy} b_{iz})^T$ the position of the attachement point B_i with respect to Frame $\{B\}$, then they can be written as

$$ {}^A a_i = \begin{bmatrix} r_A \cos(\lambda_i) & r_A \sin(\lambda_i) & 0 \end{bmatrix}^T \tag{3}$$

and

$$ {}^B b_i = \begin{bmatrix} r_B \cos(\Lambda_i) & r_B \sin(\Lambda_i) & 0 \end{bmatrix}^T \tag{4}$$

for $i = 1, 2, \ldots, 6$ where r_A and r_B represent the radii of the payload and base platforms, respectively.

We proceed to consider the vector diagram for an ith actuator given in *Fig. 4*. The length vector ${}^B q_i = (q_{ix} \ q_{iy} \ q_{iz})^T$, expressed with respect to Frame $\{B\}$ can be computed by

$$ {}^B q_i = {}^B a_i - {}^B b_i \tag{5}$$

where Vector ${}^B a_i$ and Vector ${}^B d$ describe the position of A_i and A, respectively both in terms of Frame $\{B\}$. Vector ${}^B d$ contains the Cartesian coordinates x, y, z of the origin A of Frame $\{A\}$ with respect to Frame $\{B\}$ such that

$$ {}^B d = (x \ y \ z)^T. \tag{6}$$

Let ${}^B_A R$ be the Orientation Matrix, which represents the orientation of Frame $\{A\}$ with respect to Frame $\{B\}$ and can be expressed as

$$ {}^B_A R = \begin{bmatrix} r_{11} & r_{12} & r_{13} \\ r_{21} & r_{22} & r_{23} \\ r_{31} & r_{32} & r_{34} \end{bmatrix} \tag{7}$$
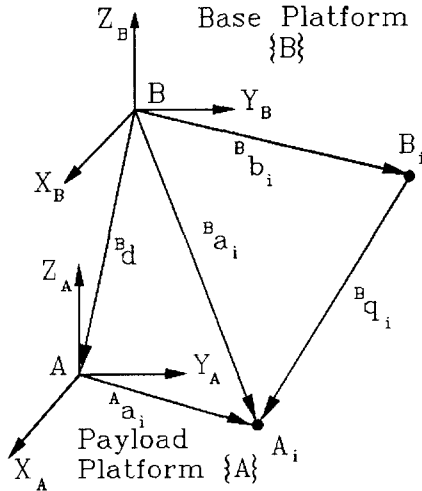
Fig. 4. Vector diagram for the ith actuator.

for $i = 1, 2, \ldots, 6$ then ${}^B a_i$ can be computed by

$$ {}^B a_i = {}^B_A R \, {}^A a_i + {}^B d. \tag{8} $$

Now substituting (8) into (5) yields

$$ {}^B q_i = {}^B_A R \, {}^A a_i + {}^B d - {}^B b_i; \quad \text{for } i = 1, 2, \ldots, 6, \tag{9} $$

which can be rewritten as

$$ {}^B q_i = \begin{bmatrix} q_{ix} \\ q_{iy} \\ q_{iz} \end{bmatrix} = \begin{bmatrix} r_{11}a_{ix} + r_{12}a_{iy} + r_{13}a_{iz} + x - b_{ix} \\ r_{21}a_{ix} + r_{22}a_{iy} + r_{23}a_{iz} + y - b_{iy} \\ r_{31}a_{ix} + r_{32}a_{iy} + r_{33}a_{iz} + z - b_{iz} \end{bmatrix}. \tag{10} $$

Furthermore, the length of Vector ${}^B q_i$, l_i can be computed from the vector components as

$$ l_i = \left(q_{ix}^2 + q_{iy}^2 + q_{iz}^2 \right)^{1/2}. \tag{11} $$

Employing (10), Equation (11) can be rewritten as

$$ l_i^2 = x^2 + y^2 + z^2 + a_{ix}^2 \left(r_{11}^2 + r_{21}^2 + r_{31}^2 \right) $$
$$ + a_{iy}^2 \left(r_{12}^2 + r_{22}^2 + r_{32}^2 \right) $$
$$ + a_{iz}^2 \left(r_{13}^2 + r_{23}^2 + r_{33}^2 \right) + b_{ix}^2 + b_{iy}^2 + b_{iz}^2 $$
$$ + 2 a_{ix} a_{iy} \left(r_{11}r_{12} + r_{21}r_{22} + r_{31}r_{32} \right) $$
$$ + 2 a_{ix} a_{iz} \left(r_{11}r_{13} + r_{21}r_{23} + r_{31}r_{33} \right) $$
$$ + 2 a_{iy} a_{iz} \left(r_{12}r_{13} + r_{22}r_{23} + r_{32}r_{33} \right) $$
$$ + 2 \left(r_{11}a_{ix} + r_{12}a_{iy} + r_{13}a_{iz} \right)(x - b_{ix}) $$
$$ + 2 \left(r_{21}a_{ix} + r_{22}a_{iy} + r_{23}a_{iz} \right)(y - b_{iy}) $$
$$ + 2 \left(r_{31}a_{ix} + r_{32}a_{iy} + r_{33}a_{iz} \right)(z - b_{iz}) $$
$$ - 2 \left(x b_{ix} + y b_{iy} + z b_{iz} \right) \tag{12} $$

for $i = 1, 2, \ldots, 6$. From the properties of the

orientation matrix we have

$$ r_{11}^2 + r_{21}^2 + r_{31}^2 = r_{12}^2 + r_{22}^2 + r_{32}^2 = r_{13}^2 + r_{23}^2 + r_{33}^2 = 1, \tag{13} $$

and

$$ r_{11}r_{12} + r_{21}r_{22} + r_{31}r_{32} = 0 $$
$$ r_{11}r_{13} + r_{21}r_{23} + r_{31}r_{33} = 0 \tag{14} $$
$$ r_{12}r_{13} + r_{22}r_{23} + r_{32}r_{33} = 0. $$

Also from (3) and (4) we note that

$$ a_{iz} = b_{iz} = 0 \tag{15} $$

and

$$ a_{ix}^2 + a_{iy}^2 + a_{iz}^2 = r_A^2 \tag{16} $$

$$ b_{ix}^2 + b_{iy}^2 + b_{iz}^2 + r_B^2 \tag{17} $$

Therefore, (12) can be simplified to

$$ l_i^2 = x^2 + y^2 + z^2 + r_A^2 + r_B^2 $$
$$ + 2 \left(r_{11}a_{ix} + r_{12}a_{iy} \right)(x - b_{ix}) $$
$$ + 2 \left(r_{21}a_{ix} + r_{22}a_{iy} \right)(y - b_{iy}) $$
$$ + 2 \left(r_{31}a_{ix} + r_{32}a_{iy} \right) z - 2 \left(x b_{ix} + y b_{iy} \right), $$

for $i = 1, 2, \ldots, 6$. \tag{18}

Equation (18) presents the solution to the inverse kinematics problem in the sense that for a given Cartesian configuration, composed of the position and orienation specified by (6) and (7), respectively, the actuator lengths l_i for $i = 1, 2, \ldots, 6$, can be computed using (18). We observe that nine variables are needed to describe the orientation of Frame $\{A\}$ in Equation (7) and six of them are redundant because only three are needed to specify an orientation [16]. There exist several ways to represent an orientation by three variables. But the most widely used one is the Euler Angles $Z - Y - X$, [17] which represent the orientation of Frame $\{A\}$, obtained after the following sequence of rotations from Frame $\{B\}$:
1. A rotation of an angle α about the z_B-axis,
2. A rotation of an angle β about the new y'_B-axis,
3. A rotation of an angle γ about the new x''_B-axis. The orientation represented by α, β, and γ is given by

$R_{zyx}(\alpha, \beta, \gamma)$

$$ = \begin{bmatrix} C\alpha C\beta & C\alpha S\beta S\gamma - S\alpha C\gamma & C\alpha S\beta C\gamma + S\alpha S\gamma \\ S\alpha C\beta & S\alpha S\beta S\gamma + C\alpha C\gamma & S\alpha S\beta C\gamma - C\alpha S\gamma \\ -S\beta & C\beta S\gamma & C\beta C\gamma \end{bmatrix} \tag{19} $$

where for compactness we have defined $S\alpha \triangleq \sin \alpha$ and $C\alpha \triangleq \cos \alpha$.

3.2. Differential Motion Analysis

First to compactly represent the dynamical equations derived in the next section, we introduce the following convention:

(a) *Cartesian Coordinates Vector:*

$$\Phi = \left(\phi_1\ \phi_2\ \phi_3\ \phi_4\ \phi_5\ \phi_6\right)^\mathrm{T}$$
$$= \left(x_1\ x_2\ x_3\ \eta_1\ \eta_2\ \eta_3\right)^\mathrm{T} = \left(x\ y\ z\ \alpha\ \beta\ \gamma\right)^\mathrm{T} \quad (20)$$

(b) *Cartesian Coordinates Velocity Vector:*

$$\dot{\Phi} = \left(\dot{\phi}_1\ \dot{\phi}_2\ \dot{\phi}_3\ \dot{\phi}_4\ \dot{\phi}_5\ \dot{\phi}_6\right)^\mathrm{T}$$
$$= \left(\dot{x}_1\ \dot{x}_2\ \dot{x}_3\ \dot{\eta}_1\ \dot{\eta}_2\ \dot{\eta}_3\right)^\mathrm{T} = \left(\dot{x}\ \dot{y}\ \dot{z}\ \dot{\alpha}\ \dot{\beta}\ \dot{\gamma}\right)^\mathrm{T} \quad (21)$$

(c) *Cartesian Translational Velocity Vector:*

$$^B v = \left(\dot{x}_1\ \dot{x}_2\ \dot{x}_3\right)^\mathrm{T} = \left(\dot{x}\ \dot{y}\ \dot{z}\right)^\mathrm{T} \quad (22)$$

(d) *Angular Velocity Vector*

$$^B \Omega = \left(\omega_1\ \omega_2\ \omega_3\right)^\mathrm{T} = \left(\omega_x\ \omega_y\ \omega_z\right)^\mathrm{T} \quad (23)$$

where ω_i is the angular velocity around the ith axis.

(e) *Moment of Inertia:*

$$\left.\begin{array}{l} I_1 = I_x \\ \quad = \text{moment of inertia around the } x\text{-axis} \\ I_2 = I_y \\ \quad = \text{moment of inertia around the } y\text{-axis} \\ I_3 = I_z \\ \quad = \text{moment of inertia around the } z\text{-axis} \end{array}\right\}$$
$$(24)$$

(f) *Cartesian Force / Torque Vector:*

$$\left(F_1\ F_2\ F_3\ F_4\ F_5\ F_6\right)^\mathrm{T} = \left(F_x\ F_y\ F_z\ M_\alpha\ M_\beta\ M_\gamma\right)^\mathrm{T}$$
$$(25)$$

where F_i is the Cartesian force (torque) along (about) the ith axis.

We proceed to compute the linear and angular velocities of the manipulator. The linear velocity of the ith link is obtained by differentiating l_i in Equation (18) with respect to time as

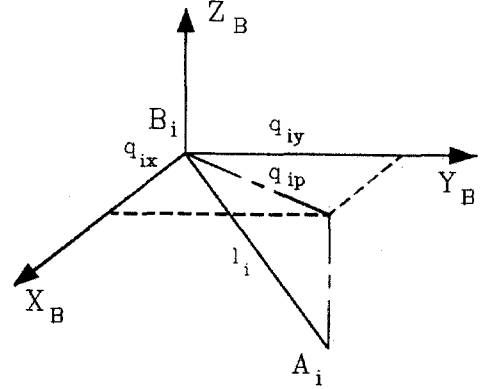$$\dot{l}_i = \sum_{k=1}^{6} c_{ik}\dot{\phi}_k \quad \text{for } i = 1,\ldots,6 \quad (26)$$

Fig. 5. Link projection on the base platform.

where

$$c_{i1} = q_{ix}/l_i \quad (27\text{a})$$

$$c_{i2} = q_{iy}/l_i \quad (27\text{b})$$

$$c_{i3} = q_{iz}/l_i \quad (27\text{c})$$

$$c_{i4} = \left[-\left(r_{21}a_{ix} + r_{22}a_{iy}\right)\left(x - b_{ix}\right)\right.$$
$$\left. + \left(r_{11}a_{ix} + r_{12}a_{iy}\right)\left(y - b_{iy}\right)\right]/l_i \quad (27\text{d})$$

$$c_{i5} = \left[C\alpha\left(r_{31}a_{ix} + r_{32}a_{iy}\right)\left(x - b_{ix}\right)\right.$$
$$\left. + S\alpha\left(r_{31}a_{ix} + r_{32}a_{iy}\right)\left(y - b_{iy}\right)\right.$$
$$\left. - \left(C\beta a_{ix} + S\beta S\gamma a_{iy}\right)z\right]/l_i \quad (27\text{e})$$

$$c_{i6} = a_{iy}\left[r_{13}\left(x - b_{ix}\right) + r_{23}\left(y - b_{iy}\right) + r_{33}z\right]/l_i. \quad (27\text{f})$$

If the angle formed between Link i and its perpendicular projection on the base platform surface is denoted by θ_i (*Fig. 5*) then

$$\tan \theta_i = q_{iz}/q_{ip} \quad (28)$$

where q_{ip}, the perpendicular projection of Link i on the base platform can be found from *Fig. 5* as

$$q_{ip} = \left(q_{ix}^2 + q_{iy}^2\right)^{1/2}. \quad (29)$$

Differentiating (28) with respect to time and utilizing (10), the *angular velocity of Link i*, $\dot{\theta}_i$ is computed by

$$\dot{\theta}_i = \sum_{k=1}^{6} t_{ik}\dot{\phi}_k \quad \text{for } i = 1,\ldots,6 \quad (30)$$

where t_{ik} is given by

$$t_{i1} = -(c_{i1}c_{i3})/q_{ip} \tag{31a}$$

$$t_{i2} = -(c_{i2}c_{i3})/q_{ip} \tag{31b}$$

$$t_{i3} = (1 - c_{i3}^2)/q_{ip} \tag{31c}$$

$$t_{i4} = -(c_{i3}c_{i4})/q_{ip} \tag{31d}$$

$$t_{i5} = \left[-(a_{ix}C\beta + a_{iy}S\beta S\gamma) + c_{i3}c_{i5} \right]/q_{ip} \tag{31e}$$

$$t_{i6} = \left[a_{iy}r_{33} - c_{i3}c_{i6} \right]/q_{ip}. \tag{31f}$$

The angular velocity vector $^B\Omega$ can be expressed in terms of the Euler angle velocities $\dot{\alpha}$, $\dot{\beta}$, and $\dot{\gamma}$ as [17]

$$^B\Omega = \begin{bmatrix} -S\alpha\dot{\beta} + C\alpha C\beta\dot{\gamma} \\ C\alpha\dot{\beta} + S\alpha C\beta\dot{\gamma} \\ \dot{\alpha} - S\beta\dot{\gamma} \end{bmatrix} \tag{32}$$

whose components can be computed by

$$\omega_k = \sum_{n=1}^{6} v_{kn}\dot{\phi}_n \quad \text{for } k = 1, 2, 3 \tag{33}$$

where v_{kn} is the (k, n) element of V defined by

$$V = \begin{bmatrix} & 0 & -S\alpha & C\alpha C\beta \\ O_{3\times3} & 0 & C\alpha & S\alpha C\beta \\ & 1 & 0 & -S\beta \end{bmatrix}. \tag{34}$$

Differentiating ω_k given in (33), the angular acceleration is obtained as

$$\dot{\omega}_k = \sum_{n=1}^{6} v_{kn}\ddot{\phi}_n + \sum_{n=1}^{6}\sum_{i=1}^{6} q_{k,nl}\dot{\phi}_n\dot{\phi}_l \tag{35}$$

where $q_{k,nl}$ denotes the $(n, 1)$ element of Q_k, for $k = 1, 2, 3$, which are given below

$$Q_1 = \begin{bmatrix} & 0 & -C\alpha & -S\alpha C\beta \\ O_{3\times3} & 0 & 0 & -C\alpha S\beta \\ & 0 & 0 & 0 \end{bmatrix}, \tag{36a}$$

$$Q_2 = \begin{bmatrix} & 0 & -S\alpha & C\alpha C\beta \\ O_{3\times3} & 0 & 0 & -S\alpha S\beta \\ & 0 & 0 & 0 \end{bmatrix}, \tag{36b}$$

$$Q_3 = \begin{bmatrix} & 0 & 0 & 0 \\ O_{3\times3} & 0 & 0 & -C\beta \\ & 0 & 0 & 0 \end{bmatrix}. \tag{36c}$$

With the results derived in the above development, we are now equipped with sufficient information to develop the equations of motion of the end-effector.

3.3. Equations of Motion

The Lagrangian formulation describes the behavior of a dynamic system in terms of work and energy stored in the system rather than in terms of forces and moments of the individual members involved [18]. Using this approach, the closed-form dynamical equations can be derived systematically in any coordinate system. The general form of Lagrangian equations of motion for an n-degree-of-freedom robot end-effector is presented by

$$F_j = d/dt(\partial L/\partial\dot{q}_j) - \partial L/\partial q_j \tag{37}$$

where the Lagrangian L is computed by

$$L = K - P, \tag{38}$$

q_j and F_j are the generalized coordinates and the generalized force/torque, respectively, K and P denote the kinetic energy and the potential energy of the end-effector, respectively.

Since no closed-form solution exists for the forward kinematics problem of the CKCM end-effector [15], we cannot express Cartesian position and orientation of the payload platform in terms of the lengths of the links. Consequently, the generalized coordinates are selected to be the Cartesian coordinates ϕ_j for $j = 1, 2, \ldots, 6$.

The total kinetic energy K of the end-effector consists of the kinetic energy created from the translational and rotational motion of the payload platform with respect to Frame $\{B\}$ and the kinetic energy produced by the rotational motion of the links about the ball joints and the translational motion of the links along the prismatic joints. Thus K can be computed by

$$K = \tfrac{1}{2}\sum_{i=1}^{6} \left(ml_{ci}^2\dot{\theta}_i^2 + m\dot{l}_{ci}^2 \right) + \tfrac{1}{2}\sum_{k=1}^{3} M\dot{x}_k^2$$

$$+ \tfrac{1}{2}\sum_{k=1}^{3} I_k\omega_k^2 \tag{39}$$

where l_{ci}, the distance between the center of gravity of the ith link and the attachment point B_i is given by

$$l_{ci} = d_0 + d_1l_i \tag{40}$$

with

$$d_0 = l_s/2 \tag{41}$$

and

$$d_1 = m_1/2m. \tag{42}$$

where

m = total mass of Link i

M = mass of the moving payload platform

m_1 = mass of the moving part of Link i

l_s = length of the stationary part of Link i.

Above for simplicity, we assume that all links are identical so that they have the same total mass and the same mass for moving parts.

Similarly, the total potential energy P of the end-effector consists of the potential energy of the payload platform and the links, and is computed by

$$P = Mgz + mg \sum_{i=1}^{6} l_{ci} \sin \theta_i \tag{43}$$

Utilizing $(37) - (43)$, we obtain after some mathematical manipulations the following equations of motion for the CKCM robot end-effector:

$$F_j = \left\{ \sum_{i=1}^{6} \left[ml_{ci}^2 \frac{\partial \dot{\theta}_i}{\partial \dot{\phi}_j} \ddot{\theta}_i + m \frac{\partial l_{ci}}{\partial \dot{\phi}_j} \ddot{l}_{ci} \right] \right.$$

$$+ \sum_{k=1}^{3} \left[M \frac{\partial \dot{x}_k}{\partial \dot{\phi}_j} \ddot{x}_k + I_k \frac{\partial \omega_k}{\partial \dot{\phi}_j} \dot{\omega}_k \right] \right\}$$

$$+ \left\{ \sum_{i=1}^{6} \left[ml_{ci}^2 \dot{\theta}_i \frac{d}{dt} \left(\frac{\partial \dot{\theta}_i}{\partial \dot{\phi}_j} \right) + ml_{ci} \frac{d}{dt} \left(\frac{\partial \dot{l}_{ci}}{\partial \dot{\phi}_j} \right) \right. \right.$$

$$+ 2ml_{ci} \dot{\theta}_i \frac{\partial \dot{\theta}_i}{\partial \dot{\phi}_j} \dot{l}_{ci} - ml_{ci} \frac{\partial l_{ci}}{\partial \phi_j} \dot{\theta}_i^2$$

$$\left. - ml_{ci}^2 \dot{\theta}_i \frac{\partial \dot{\theta}_i}{\partial \phi_j} - ml_{ci} \frac{\partial \dot{l}_{ci}}{\partial \phi_j} \right]$$

$$\left. + \sum_{k=1}^{3} \left[I_k \omega_k \frac{d}{dt} \left(\frac{\partial \omega_k}{\partial \dot{\phi}_j} \right) - I_k \omega_k \frac{\partial \omega k}{\partial \phi_j} \right] \right\}$$

$$+ \left\{ \sum_{i=1}^{6} \left[mg \frac{\partial l_{ci}}{\partial \phi_j} \sin \theta_i + mgl_{ci} \cos \theta_i \frac{\partial \theta_i}{\partial \phi_j} \right] \right.$$

$$\left. + Mg \frac{\partial z}{\partial \phi_j} \right\}$$

for $j = 1, 2, \ldots, 6$. $\tag{44}$

Equation (44) represents the relationship between the Cartesian forces/torques F_j for $j =$

$1, 2, \ldots, 6$ applied to the moving platform and the Cartesian position and orientation of the payload platform ϕ_j for $j = 1, 2, \ldots, 6$. Our ultimate goal is to obtain closed-form dynamic equations which are presented in an explicit input-output form where F_j and ϕ_j for $j = 1, 2, \ldots, 6$ are considered as input and outputs, respectively.

We proceed to compute the partial derivative terms in (44) and express them in terms of ϕ_j, $\dot{\phi}_j$, and $\ddot{\phi}_j$, for $j = 1, 2, \ldots, 6$ which yields

$$F_j = \sum_{m=1}^{6} D_{jm} \ddot{\phi}_m + \sum_{m=1}^{6} \sum_{n=1}^{6} H_{jmn} \dot{\phi}_m \dot{\phi}_n + G_j \tag{45}$$

for $j = 1, 2, \ldots, 6$, which can be decomposed into the following terms:

(a) *Inertial terms:*

$$D_{jm} = \sum_{i=1}^{6} \left[ml_{ci}^2 t_{ij} t_{im} + d_1^2 c_{ij} c_{im} + e_{im} \right], \tag{46}$$

where e_{im} denotes the (m, n) element of E given by

$$E = \begin{bmatrix} M & 0 & 0 & 0 & I_1 v_{ij}(-S\alpha) & I_1 v_{1j}(C\alpha C\beta) \\ 0 & M & 0 & 0 & I_2 v_{2j}(C\alpha) & I_2 v_{2j}(S\alpha C\beta) \\ 0 & 0 & M & I_3 v_{3j} & 0 & I_3 v_{3j}(-S\beta) \\ \hline & & & O_{3 \times 6} & & \end{bmatrix}. \tag{47}$$

(b) *Centrifugal and Coriolis terms:*

$$H_{jmn} = \sum_{i=1}^{6} m \left[l_{ci}^2 t_{ij} h_{mn} + d_1^2 c_{ij} s_{mn} + l_{ci}^2 t_{im} h_{jn} \right.$$

$$+ d_1 c_{im} s_{jn} + 2 d_1 l_{ci} t_{ij} t_{im} c_{in}$$

$$- d_1 l_{ci} c_{ij} t_{im} t_{in} - l_{ci}^2 t_{im} h_{nj}$$

$$\left. - d_1^2 c_{im} s_{nj} \right]$$

$$+ \sum_{k=1}^{3} \left[I_k v_{kj} q_{k,mn} - I_k v_{km} p_{k,nj} \right] \tag{48}$$

where

$$h_{jn} = \left[q_{ip}^2 \left(u_{jn} c_{i3} + c_{ij} u_{3n} - 2c_{ij} c_{i3} c_{in} \right) \right.$$

$$\left. - l_i \left(c_{in} l_i - q_{iz} u_{3n} \right) \right], \tag{49}$$

$$s_{jn} = (u_{jn} - c_{ij} c_{in})/l_i, \tag{50}$$

$p_{k.nj}$ and u_{jn} are the (n, j) and (j, n) elements of P_k and U, respectively, given by

$$P_1 = \begin{bmatrix} O_{3 \times 6} \\ \hline & -C\alpha & S\alpha C\beta \\ O_{3 \times 4} & 0 & -C\alpha C\beta \\ & 0 & 0 \end{bmatrix}, \qquad (51a)$$

$$P_2 = \begin{bmatrix} O_{3 \times 6} \\ \hline & -S\alpha & C\alpha C\beta \\ O_{3 \times 4} & 0 & -S\alpha S\beta \\ & 0 & 0 \end{bmatrix}, \qquad (51b)$$

$$P_3 = \begin{bmatrix} O_{3 \times 6} \\ \hline & 0 \\ O_{3 \times 5} & -C\alpha \\ & 0 \end{bmatrix}, \qquad (51c)$$

and

$$U = \begin{bmatrix} 1 & 0 & 0 & -(a_{ix}r_{21} + a_{iy}r_{22}) & (a_{ix}C\alpha S\beta - a_{iy}r_{32}C\alpha) & a_{iy}r_{13} \\ 0 & 1 & 0 & (a_{ix}r_{11} + a_{iy}r_{12}) & S\alpha(a_{ix}r_{31} + a_{iy}r_{32}) & a_{iy}r_{23} \\ 0 & 0 & 1 & 0 & -(a_{ix}C\beta + a_{iy}S\beta S\gamma) & a_{iy}r_{33} \end{bmatrix}. \qquad (52)$$

(c) *Gravity terms:*

$$G_j = \sum_{i=1}^{6} \left[mgc_{ij} \sin \theta_i + mgl_{ci}t_{ij} \cos \theta_i \right] + Mg\mu. \qquad (53)$$

where

$$\mu = \partial z / \partial \Phi_j = \begin{cases} 1 & \text{if } j = 3 \\ 0 & \text{if } j \neq 3. \end{cases} \qquad (54)$$

Reader who interests in the detailed development of the above equations can refer to [18].

4. Computer Simulation Study

In order to gain some insight of the manipulator characteristics, the kinematics and dynamics developed in previous sections are now studied using computer simulation. Simulation study of the CKCM end-effector is performed in two parts. In the first part of the study, since robotic assembly often occurs in a slow motion mode, we first study the dynamics of the end-effector in this case. In particular, we will show that for slow motion, the derived dynamical equations can be greatly simplified. In the second part, we will study the effects of system parameters on the dynamics so that optimization of the system parameters for the hardware implementation of the end-effector can be achieved.

In the above computer simulation studies, computer programs written in Fortran, software packages such as System Simulation Language (SYSL) and Matlab will be employed to study the case in which the end-effector is to track an ellipse on a horizontal plane below the base platform, which is specified by [*Fig. 6*]

$$(x/5)^2 + (y/2.5)^2 = 1 \text{ (in cm).} \qquad (55)$$

4.1. Simplification of the Equations of Motion

The computer simulation study is described by the block diagram given in *Fig. 7*. In the figure, first the actuator lengths, as joint variables required for tracking the Cartesian path specified by (55) are computed using the inverse kinematic solution given by (18). The required actuator lengths are then applied to the dynamic equations
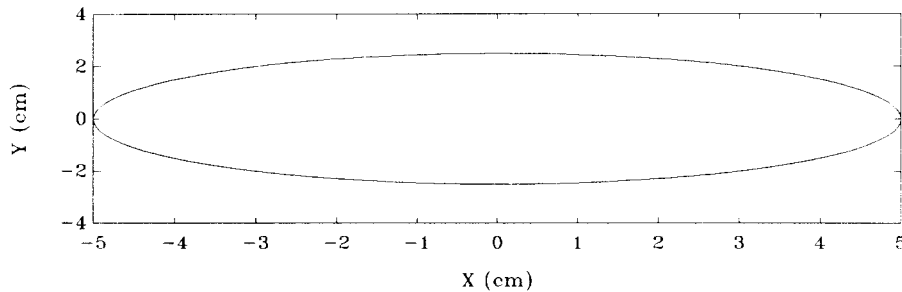

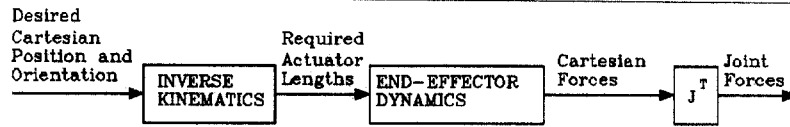Fig. 6. The path to be tracked by the end-effector.

Fig. 7. Block diagram of the computer simulation studies.

given by (45) to find the Cartesian forces, which in turn are transformed to corresponding joint forces via the Jacobian transpose by

$$\tau_j = J^T F_j \quad \text{for } j = 1, 2, \ldots, 6. \tag{56}$$

Most existing CKCM manipulators with ball-screw actuators and driven by either dc motors or stepper motors have a linear velocities range from 1.5 cm/sec to about 8.5 cm/sec [14], [9]. Therefore, using the procedure shown in Fig. 5, we compute the actuating forces, the inertial forces, the centrifugal and Coriolis forces, and the gravity forces for the cases in which the maximum actuator velocities fall between 0.7 cm/sec to 17 cm/sec in order to cover the maximum actuator velocities limited by the applied motors as specified above. The computation results for two extreme velocities 0.7 cm/sec and 17 cm/sec are tabulated in Tables 1 and 2, respectively.

Table 1 shows that the end-effector needs 3 seconds to track the desired path with a maximum velocity of 0.7 cm/sec where in Table 2, 0.5 seconds are required for the maximum velocity of 17 cm/sec. In both tables, we observe that the force

contribution from the Coriolis and centrifugal terms remains about 1% of the toral forces while the contribution from the inertial terms jumps from 1% in Table 1 to about 100% in Table 2. Since the centrifugal and Coriolis effects are very minimal, the desired dynamical equations in (45) can be simplified by neglecting the centrifugal and Coriolis terms such that

$$F_j = \sum_{m=1}^{6} D_{jm} \ddot{\phi}_m + G_j \tag{57}$$

which ensures that the maximum error in total force computation is about 1%. The simplified model (57) will be employed in the second part of the simulation study. System parameters used in the above simulation are given below:

$$m = 20 \text{ kg}, \ m_1 = 4.4 \text{ kg}, \ M = 30 \text{ kg}, \ r_A = 0.7 \text{ m},$$

$$r_B = 0.8 \text{ m}, \ \theta_A = 30°, \ \theta_B = 94°. \tag{58}$$

4.2. Effects of the System Parameters

In this section, computer simulations are performed to study the effects of the system parame-

Table 1 Comparison between Dynamic Forces

Vmax = 0.7 cm/sec

Time (sec)	Inertial	Velocity Products (Forces in Newton)	Gravity	Total
0.0	0.000	0.000	$2.096 \times 10^{+1}$	$2.096 \times 10^{+1}$
0.5	-2.827×10^{-1}	-1.869×10^{-3}	$1.972 \times 10^{+1}$	$1.944 \times 10^{+1}$
1.0	-2.403×10^{-1}	-1.743×10^{-3}	$1.657 \times 10^{+1}$	$1.632 \times 10^{+1}$
1.5	-1.744×10^{-1}	-1.286×10^{-3}	$1.183 \times 10^{+1}$	$1.165 \times 10^{+1}$
2.0	-9.140×10^{-2}	-6.475×10^{-4}	5.973	5.881
2.5	4.270×10^{-4}	-5.454×10^{-5}	-4.287×10^{-1}	-4.283×10^{-1}
3.0	9.220×10^{-2}	2.735×10^{-4}	-6.778	-6.685

Table 2 Comparison between Dynamic Forces

Vmax = 17 cm/sec

Time (sec)	Inertial	Velocity Products (Forces in Newton)	Gravity	Total
0.0	0.000	0.000	$2.096 \times 10^{+1}$	$2.096 \times 10^{+1}$
0.1	$-3.696 \times 10^{+1}$	-2.616×10^{-1}	5.973	$-3.125 \times 10^{+1}$
0.2	$9.671 \times 10^{+1}$	-9.213×10^{-2}	$-1.701 \times 10^{+1}$	$7.961 \times 10^{+1}$
0.3	$9.687 \times 10^{+1}$	-7.359×10^{-1}	$-1.689 \times 10^{+1}$	$7.924 \times 10^{+1}$
0.4	$-3.661 \times 10^{+1}$	7.624×10^{-2}	6.827	$-2.970 \times 10^{+1}$
0.5	$-1.198 \times 10^{+2}$	-6.558×10^{-1}	$2.096 \times 10^{+1}$	$-9.950 \times 10^{+1}$

ters on the end-effector dynamics. The four study cases presented below investigate the case in which the end-effector tracks the path specified in (55) and unless otherwise specified, the system parameters given in (58) are used.

Case 1. Effect of the total mass of the links
Keeping all system parameters as in (58), except the link mass m, computer simulations are per-formed to compute the actuating forces in six links for various link masses. The results in *Fig. 8*, show that the forces are increased with increasing link masses.

Case 2. Effect of the link centroid
While keeping all system parameters as in (58), except m_1 which is changed in order to change the centroid l_{ci}, the distance between the center of
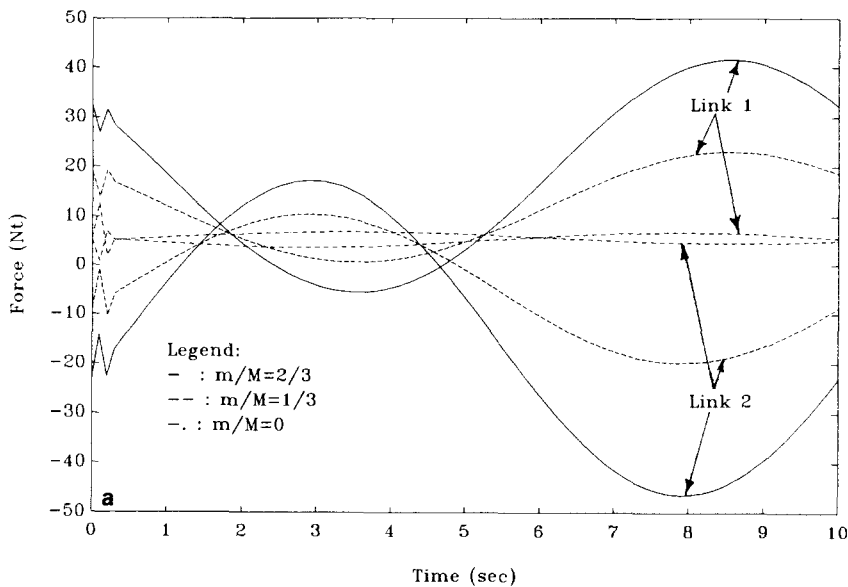
Figs. 8a–c. The effect of link masses on actuating forces.
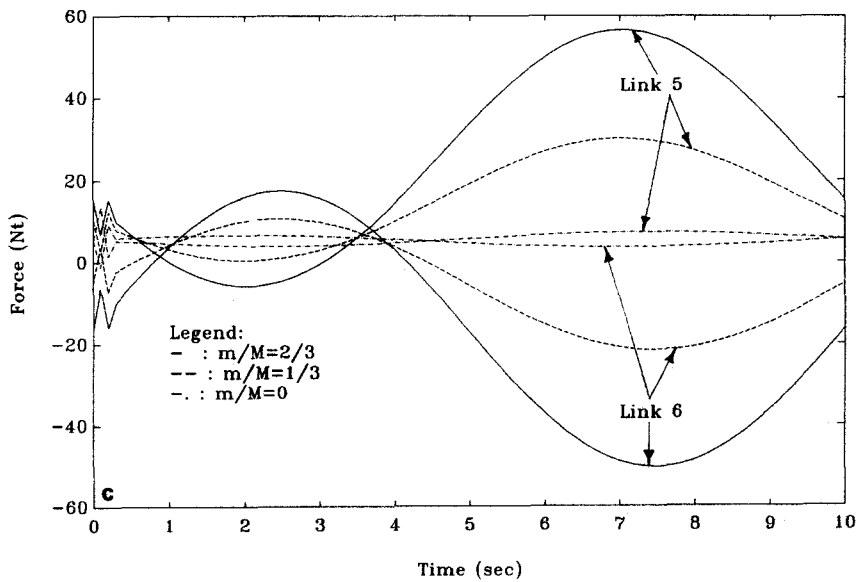(8a). For Links 1 and 2.
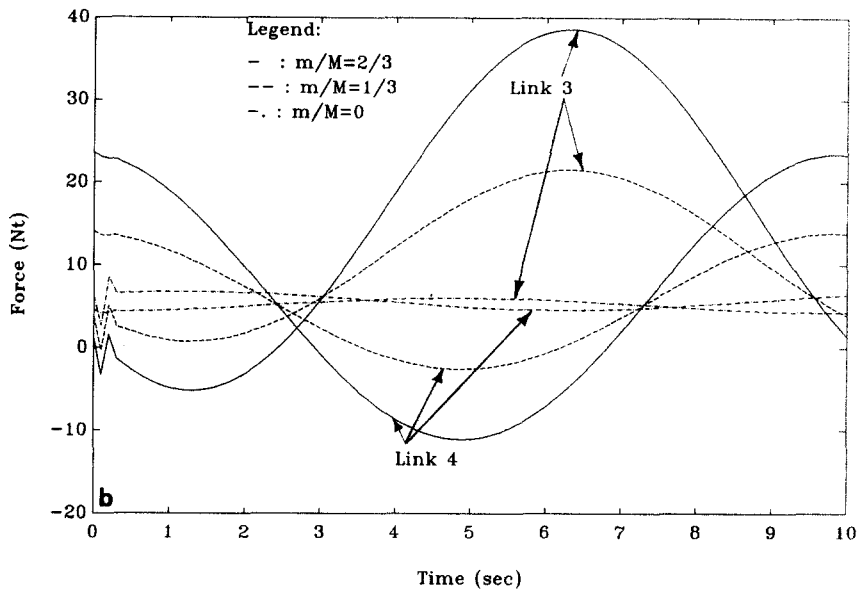
(8b). For Links 3 and 4.

mass of the link and the attachment point B_i, as described in (40) and (42), we conduct computer simulations to study the effects of l_{ci} on the end-effector dynamics. The results of the study presented in *Fig. 9* show that moving the link

centroid closer to the base frame reduces the actuating forces in the links.

Case 3. Effect of the angles between ball joints A_i Keeping all system parameters as in (58), except θ_A, the angle between ball joints A_i, computer

(8c). For Links 5 and 6.
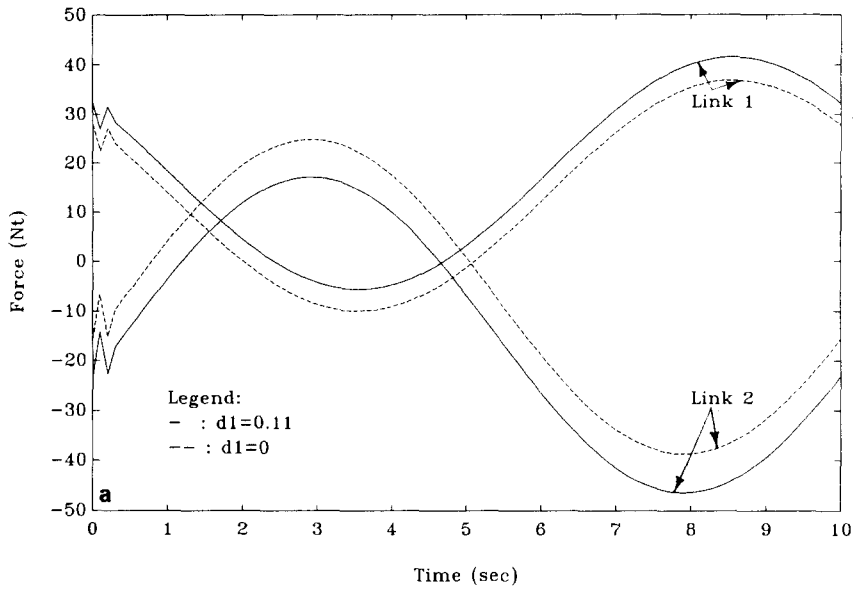
Figs. 9a–c. The effect of center of mass on actuating forces.
(9a). For Links 1 and 2.

simulations are performed to compute the actuating forces in six links for various θ_A. The simulation results reported in *Fig. 10* show that reducing θ_A reduces the actuating forces.

Case 4. Effect of the angles between ball joints B_i
Keeping all system parameters as in (58), except θ_B, the angle between ball joints B_i, computer simulations are conducted to compute the actu-
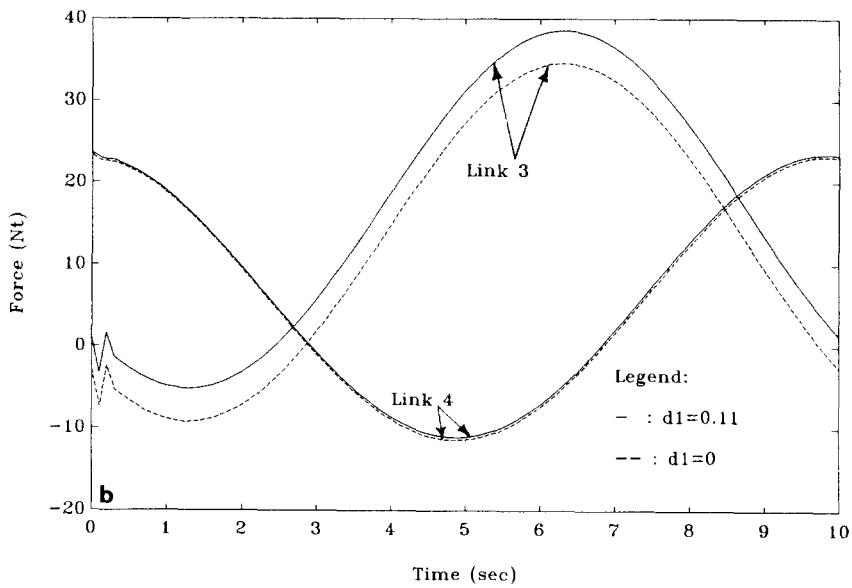
(9b). For Links 3 and 4.
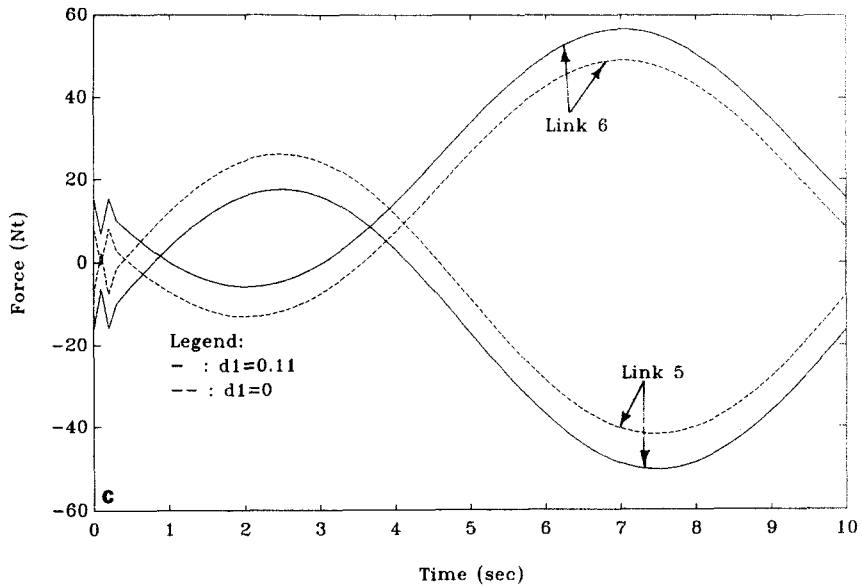
(9c). For Links 5 and 6.

ating forces in six links for various θ_B. The results in *Fig. 11* show that increasing θ_B will reduce the actuating forces.
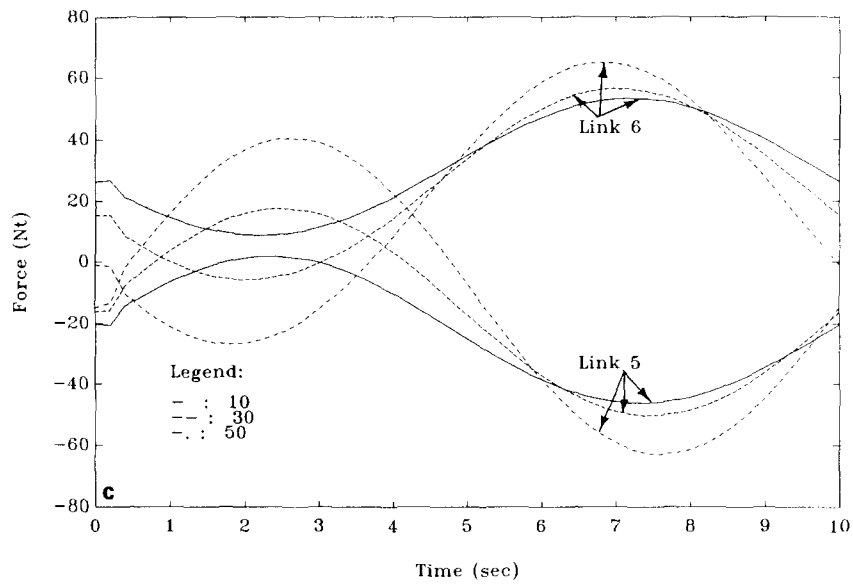
The hardware requirements for the implementation of the end-effector in terms of power, weight and sizes of the actuators can be optimized by the
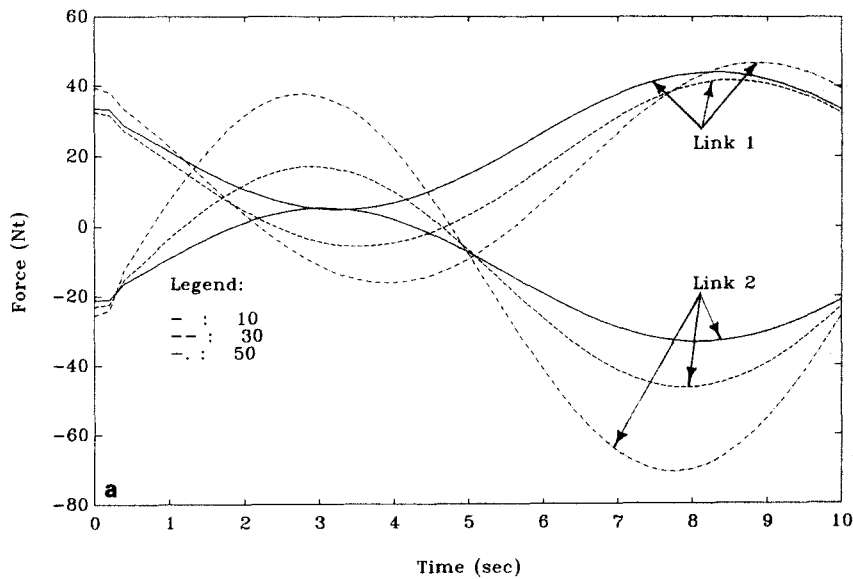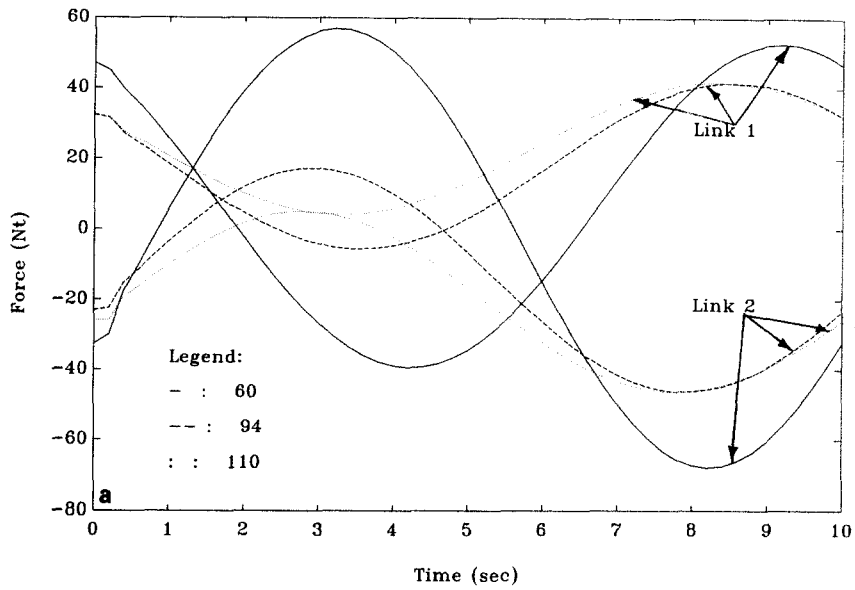

Figs. 10a–c. The effect of angle between ball joints A_i on actuating forces.
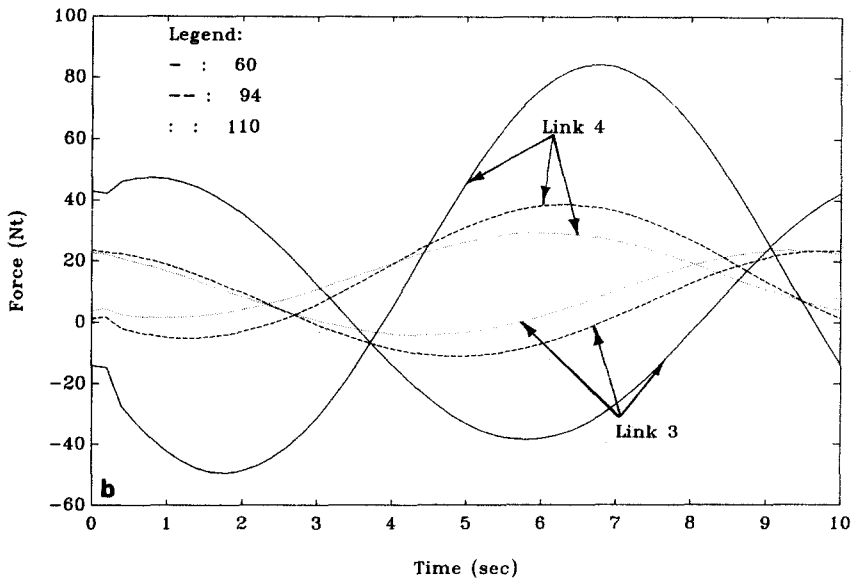(10a). For Links 1 and 2.
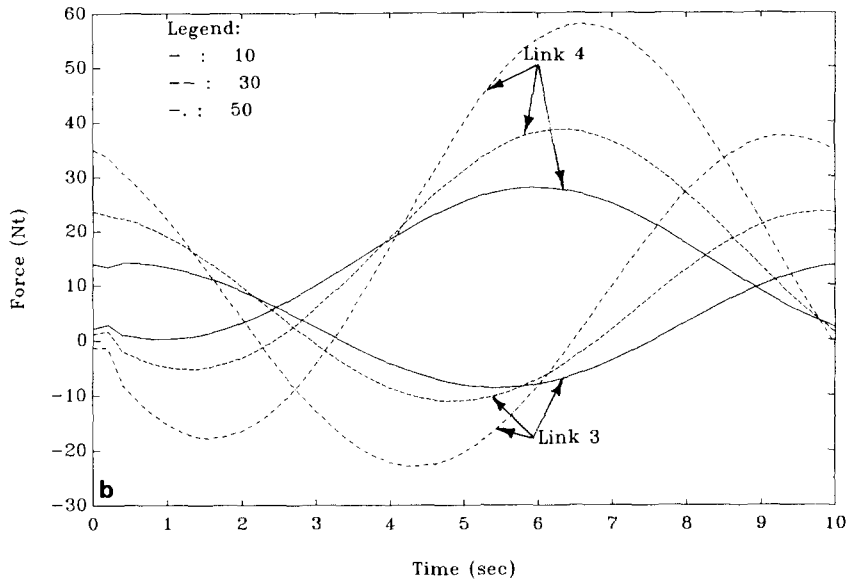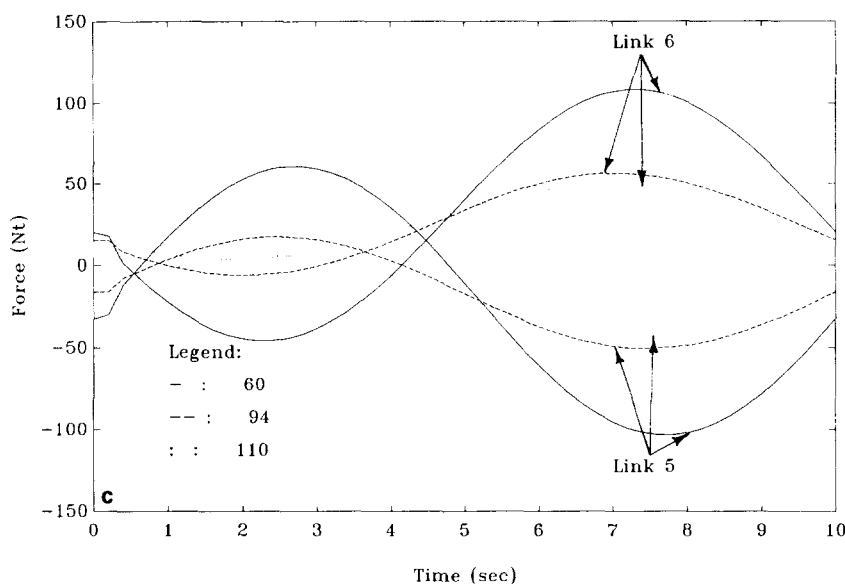
(10b). For Links 3 and 4.

(10c). For Links 5 and 6.

Figs. 11a–c. The effect of angle between ball joints B_i on actuating forces.
(11a). For Links 1 and 2.

(11b). For Links 3 and 4.

(11c). For Links 5 and 6.

following general guideline obtained through the above simulation studies:

1. The power, weights and sizes of the end-effector actuators can be minimized if the link masses are reduced or the link centroids are moved closer to the base platform.

2. Appropriate selection of the angles θ_A and θ_B can minimize the power, weights and sizes of the end-effector actuators. Optimization of actuators can be achieved if we keep θ_A as small as possible and θ_B as large as possible.

5. Conclusions

In this paper, we presented the dynamical analysis of a 6 DOF robot end-effector mounted to the slave arms of a dual-arm telerobot system to perform telerobotic assembly of NASA hardwares in space. The end-effector was designed using the concept of closed-kinematic chain mechanism and is a modified version of the Stewart platform [2]. A closed-form solution for the inverse kinematic problem was obtained so that actuator lengths as joint variables can be computed for a given Cartesian configuration composed of position and orientation. Using the Lagrangian approach and selecting the Cartesian position and orientation as

the generalized coordinates, we derived the equations of motion for the end-effector. Based on performed computer simulation studies which showed that the centrifugal and Coriolis effects are negligible in the dynamical equations, we simplified the derived equations of motion while assuring that the force computation errors caused by the simplication are under 1% of the total force. Also through computer simulation study of the effects of system parameters on the end-effector dynamics, a general guideline was provided to minimize the power requirements, weights and sizes of end-effector actuators. Kinematic and dynamical equations derived in this paper can be applied to special cases of 3 DOF manipulator [13] and 2 DOF end-effector [14]. Workspace and forward kinematic problems of this end-effector were investigated in [15]. Future research can be extended to study feedback control schemes such as adaptive [20] or learning for the trajectory and/or force control [19] of the 6 DOF end-effector.

Acknowledgments

Reference

[1] JPL, Telerobotics project plan, Jet Propulsion Laboratory, JPL D-5692 (August 1988).
[2] D. Stewart, A platform with six degrees of freedom, Proc. Institute of Mechanical Engineering, 180, part 1, No. 5 (1965–1966) 371–386.
[3] J.E. Dieudonne et al., An actuator extension transformation for a motion simulator and an inverse transformation applying Newton–Raphson's method, NASA Technical Report D-7067 (1972).
[4] K.H. Hunt, Kinematic geometry of mechanisms, Oxford University, London (1978).
[5] E.F. Fichter and E.D. MacDowell, A novel design for a robot arm, ASME Int. Computer Technology Conference, San Francisco (1980) 250–256.
[6] K.H. Hunt, Structural kinematics of in-parallel actuated robot arms, Trans. ASME, J. Mech., Transmis., Automa. in Des., 105 (1983) 705–712.
[7] E.F. Fichter, A Stewart platform-based manipulator: General theory and practical construction, Int. Journal of Robotics Research, (1986) 157–182.
[8] K. Sugimoto and J. Duffy, Application of linear algebra to screw systems, Mech. Mach. Theory, 17, No. 1 (1982) 73–83.
[9] T. Premack et al., Design and implementation of a compliant robot with force feedback and strategy planning software, NASA Technical Memorandum 86111 (1984).
[10] D.C. Yang and T.W. Lee, Feasibility study of a platform type of robotic manipulators from a kinematic viewpoint, Trans. ASME J. Mechanisms, Transmissions, and Automation in Design, 106 (1984) 191–198.
[11] W.Q.D. Do and D.C.H. Yang, Inverse dynamics of a platform type of manipulating structure, ASME Design Engineering Technical Conference, Columbus, Ohio, (1986) 1–9.
[12] K. Sugimoto, Kinematic and dynamic analysis of parallel manipulators by means of motor algebra, ASME J. Mechanisms, Transmissions, and Automation in Design, (1986) 1–5.
[13] K.M. Lee and D.K. Shah, Dynamic analysis of a three-degrees-of-freedom in-parallel actuated manipulator, IEEE J. Robotics and Automation, 4, No. 3 (1988) 361–367.
[14] C.C. Nguyen, F.J. Pooran, and T. Premack, Trajectory control of robot manipulator with closed-kinematic chain mechanism, Proc. 20th Southeastern Symposium on System Theory, North Carolina (1988) 454–458.
[15] C.C. Nguyen and F.J. Pooran, Kinematic analysis and workspace determination of a 6 DOF CKCM robot end-effector, J. Mechanical Working Technology 20 (1989) 283–294.
[16] K.S. Fu et al., Robotics: Control, Sensing, Vision, and Intelligence (McGraw-Hill, New York, 1987).
[17] H. Asada and J.J.E. Slotine, Robot Analysis and Control (John Wiley and Sons, 1986).
[18] F.J. Pooran, Dynamics and control of robot manipulators with closed-kinematic chain mechanism, Ph.D. Dissertation, Mechanical Engineering, Catholic University of America, Washington, DC (1989).
[19] C.C. Nguyen, F.J. Pooran and T. Premack, Modified hybrid control of Robot manipulator for high precision assembly operations, Proc. ISMM Int. Conference on Computer Application in Design, Simulation and Analysis, Honolulu, Hawai (February 1988) 191–195.
[20] C.C. Nguyen, and F.J. Pooran, Joint-space adaptive control of robot end-effectors performing slow and precise motions, Proc. 21st Southeastern Symposium on System Theory, FL (March 1989) 547–552.